Available online at https://jcupt.bupt.edu.cn

The Journal of China Universities of Posts and Telecommunications

April 2025, 32(2): 101 – 110

Performance study of wavelength diversity OFDM underwater wireless optical communication system

He Fengtao, Wang Ruina (✉), Guo Shaohui, Liu Runan, Yang Yi, Zhang Jianlei

School of Electronic Engineering, Xi'an University of Posts and Telecommunications, Xi'an 710121, China

Abstract

The performance of underwater wireless optical communication (UWOC) system is degraded due to the influence of seawater transmission path loss, ocean turbulence effect, and pointing error during the transmission of optical signals. In order to solve this problem, an orthogonal frequency division multiplexing (OFDM) UWOC system composite channel model based on wavelength diversity was established, and the analytical expressions for the outage probability and the average symbol error rate (SER) of the system were derived. The system performance of wavelength diversity UWOC is investigated under different pointing errors, number of subcarriers, and maximum ratio combining (MRC) and equal gain combining (EGC) schemes. The results show that the performance of the UWOC system using the wavelength diversity technique is significantly improved. Compared with the no-diversity system, a diversity order of 3 reduces the outage probability from 10^{-3} to the order of 10^{-8} and the average SER from 10^{-2} to 10^{-7}. A smaller pointing error reduces the outage probability of the system. Additionally, a larger ratio of beam width to receiver aperture also decreases the outage probability. Increasing the number of subcarriers will increase the system's average symbol error rate.

Keywords underwater wireless optical communication (UWOC), pointing error, strong ocean turbulence, wavelength diversity, orthogonal frequency division multiplexing (OFDM)

1 Introduction

UWOC has gained significant attention due to its advantages of high transmission rate, low latency, wider bandwidth, and higher security[1]. However, due to the influence of seawater transmission path loss, optical signal attenuation, and ocean turbulence effect[2] in the process of optical signal transmission can result in flickering of light intensity at the receiver. Additionally, the pointing errors may cause beam drift, which degrades the quality of system communications.

In recent years, many turbulence models adapted to different turbulence intensities have been proposed by researchers. The lognormal distribution model[3] is only suitable for weak turbulence conditions, while the Gamma-Gamma turbulence model[4] provides the best-fit irradiance statistics for medium-strong turbulence conditions. The *K*-distribution model is better suited for strong turbulence conditions. To mitigate channel fading, commonly employed techniques include diversity techniques, relay assistance, modulation schemes, and aperture averaging. There are three

Special Issue: The 27th Annual Meeting of The China Association for Science and Technology

Corresponding author: Wang Ruina, E-mail: wangruina0@163.com

DOI: 10.19682/j.cnki.1005-8885.2025.0012

common diversity techniques: spatial diversity, wavelength diversity, and frequency diversity. Wavelength diversity[5] involves transmitting multiple data copies at different wavelengths to overcome the turbulence effects. Wang et al.[6] proposed a serial relay OFDM free-space optical communication system based on wavelength diversity and evaluated the performance of the system under the combined effects of transmission path loss, atmospheric turbulence, and pointing errors using an exponential Weibull channel model. He et al.[7] investigated wavelength diversity based UWOC system using on-off keying (OOK) modulation over a joint fading channel with Gamma-Gamma turbulence to analyze the outage probability and average bit error rate (BER) of the system. Nayak et al.[8] investigated three modulation schemes in UWOC: quadrature phase shift keying (QPSK), dual-polarization QPSK (DP-QPSK), and 4-quadrature amplitude modulation (4-QAM). They compared the system performance across multiple metrics, including the maximum quality factor, minimum BER, spectral efficiency, and eye diagram. Mohammed et al.[9] studied the enhancement of UWOC performance using multiple-input multiple-output (MIMO) configurations combined with DP-OFDM and QPSK techniques, achieving a maximum communication distance of up to 230 m and BER of 10^{-8}. Wavelength diversity has been extensively studied in free space optical (FSO) communication systems, while its application in seawater channels remains relatively unexplored.

Compared with OOK modulation, OFDM can reduce or eliminate inter-symbol interference. Therefore, the performance of OFDM UWOC systems with wavelength diversity is evaluated under the influence of three key factors: seawater path loss, ocean turbulence effect, and pointing errors. At the receiver, MRC and EGC techniques are employed, and the analytical expressions are deduced on the outage probability and the average SER of the system. The impact of pointing errors and beam width on the outage probability, as well as the effects of diversity order, subcarrier number, and the two combining techniques on the average SER are analyzed.

2 System model

The transmission model of OFDM UWOC with wavelength diversity is shown in Fig. 1. In this system, the mapping method used is QPSK. Wavelength diversity is achieved by transmitting the same signals simultaneously across multiple wavelengths from a composite transmitter. After traversing the composite channel, which is influenced by attenuation, oceanic turbulence, and pointing errors, each receiver individually detects the signal corresponding to its assigned wavelength. These signals are finally merged at the combining unit.

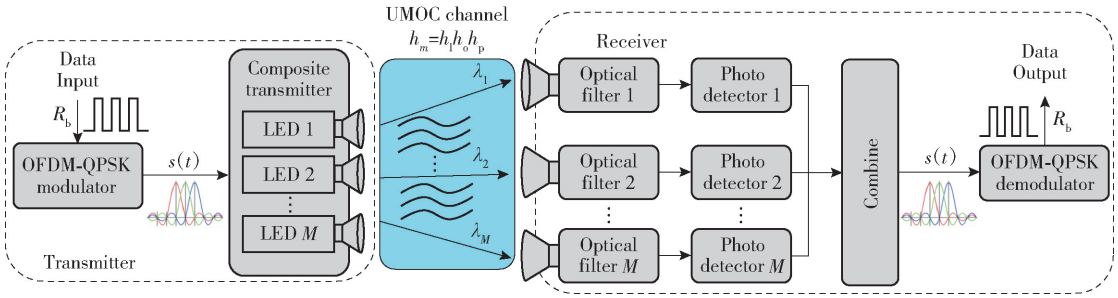

Fig. 1 OFDM UWOC system based on wavelength diversity under QPSK modulation

It is assumed that there is additive Gaussian white noise (AGWN) in the channel and composite transmitters using M different wavelengths. These transmitters simultaneously send signals carrying identical data, which are transmitted through the turbulence channel model and are finally received by the receivers at M specific wavelengths. For the mth receiver, the received signal can be expressed as[10]

$$y_m = h_m x_m \rho + z_m; \quad m = 1, 2, \ldots, M \tag{1}$$

where h_m denotes the fading factor of the mth composite

channel, x_m is the OFDM signal after modulation at the transmitter side, ρ is the receiver responsivity, and z_m denotes the AGWN with zero mean and variance $N_0/2$, where N_0 is the noise power spectral density.

OFDM is a multi-carrier modulation technique that transmits signals in parallel over multiple subcarriers. Assuming there are N sub-signals, the time-domain expression of an individual sub-signal is given as[11]

$$s_n(t) = a_n \cos(2\pi f_n t + \phi_n); \quad 0 \leqslant n \leqslant N-1 \tag{2}$$

where f_n is the frequency of the nth subcarrier, ϕ_n is the initial phase, t denotes time, and a_n is the amplitude. The time-domain expression of an OFDM symbol is the sum of these N sub-signals, which can be expressed in complex form as

$$s(t) = \mathrm{Re}\left\{ \sum_{n=0}^{N-1} A_n e^{j2\pi f_n t} \right\} \tag{3}$$

where $A_n = a_n \cos \phi_n + j a_n \sin \phi_n$ is the complex envelope of the modulated signal on the nth subcarrier, generally obtained by modulating the baseband signal through QAM or phase shift keying (PSK) schemes. In QPSK, each symbol carries two bits of information, resulting in four possible phase states, 0°, 90°, 180°, and 270°.

3 Channel model

3.1 Absorption and scattering

The propagation of a beam underwater induces absorption and scattering effects between photons and seawater particles, which attenuate the average irradiance of the beam. The path loss of optical signal transmission in seawater can be expressed as

$$h_l = e^{-c(\lambda)L} \tag{4}$$

where L is the transmission distance of the optical signal underwater. The total attenuation coefficient is represented as[12]

$$c(\lambda) = a(\lambda) + b(\lambda) \tag{5}$$

where $a(\lambda)$ and $b(\lambda)$ denote the absorption and scattering coefficients, respectively. These coefficients vary with the source wavelength λ and the type of water body. The total attenuation coefficients of optical signals of different wavelengths in offshore water quality are shown in Fig. 2. In offshore water, the chlorophyll concentration is 0.3 mg/m^3 and the non-pigmented suspended particle concentration is 0.8 mg/dm^3[13]. From Fig. 2, optical signals between 550 – 590 nm have lower total attenuation coefficients during transmission, and the minimum total attenuation coefficient is observed at 570 nm.

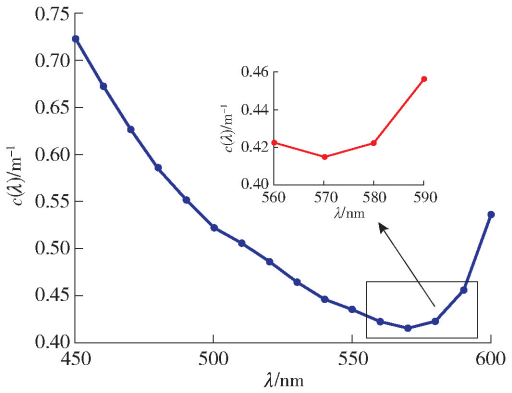

Fig. 2 Total attenuation coefficient of light signals of different wavelengths in offshore water quality

Therefore, in this paper, 560 nm, 570 nm, and 580 nm are chosen as the working wavelengths for the transmission signal of the 3rd-order wavelength diversity system. For the 2nd-order wavelength diversity system, 560 nm and 570 nm are selected, while 570 nm is used for the no-wavelength diversity system. Table 1 shows the offshore attenuation coefficients for the optical wavelengths selected for the diversity system.

Table 1 Offshore attenuation coefficients corresponding to the wavelengths of light selected for diversity

λ/nm	$a(\lambda)$/m^{-1}	$b(\lambda)$/m^{-1}	$c(\lambda)$/m^{-1}
560	0.184 5	0.237 9	0.422 4
570	0.181 3	0.233 7	0.415 0
580	0.192 6	0.229 7	0.422 3

3.2 Gamma-Gamma distribution turbulence model

In this paper, the Gamma-Gamma distribution is adopted to model the turbulence conditions. The irradiance power density function (PDF) of the signal at the receiver end after transmission through this channel follows the Gamma-Gamma statistical distribution[14].

$$f_{h_o}(h_o)=\frac{2(\alpha\beta)^{\frac{\alpha+\beta}{2}}}{\Gamma(\alpha)\Gamma(\beta)}(h_o)^{\frac{\alpha+\beta}{2}-1}\mathrm{K}_{\alpha-\beta}(2\sqrt{\alpha\beta h_o}) \quad (6)$$

where $\mathrm{K}_{\alpha-\beta}(\cdot)$ is the $(\alpha-\beta)$-order modified Bessel function of the second kind, $\Gamma(\cdot)$ is the Gamma function. α and β are the large-scale and small-scale light wave scintillation coefficients[15], respectively, are defined as

$$\alpha=\left[\exp\left(\frac{0.196\sigma_l^2}{(1+0.18d^2+0.186\sigma_l^{\frac{12}{5}})^{\frac{7}{6}}}\right)-1\right]^{-1} \quad (7)$$

$$\beta=\left[\exp\left(\frac{0.204\sigma_l^2(1+0.23\sigma_l^{\frac{12}{5}})^{-\frac{5}{6}}}{1+0.9d^2+0.207d^2\sigma_l^{\frac{12}{5}}}\right)-1\right]^{-1} \quad (8)$$

where $d=\sqrt{kD^2/(4L)}$, the Rytov variance under ocean turbulence is $\sigma_l^2=1.23C_\mathrm{n}^2k^{7/6}L^{11/6}$. $k=2\pi/\lambda$ is the wave number, λ is the wavelength, D is the receiving aperture size, and C_n^2 is the refractive index structure constant[16].

$$C_\mathrm{n}^2=8\pi k^{-\frac{7}{6}}L^{-\frac{11}{6}}\mathrm{Re}\left\{\int_0^L\mathrm{d}z\int_{-\infty}^{\infty}\mathrm{d}k_x\int_{-\infty}^{\infty}\mathrm{d}k_y\cdot[P(z,k_x,k_y)P(z,-k_x,-k_y)+|P(z,k_x,k_y)|^2\Phi_\mathrm{n}(k)]\right\} \quad (9)$$

where z is the beam propagation direction, k_x and k_y denote the spatial frequency components in the x and y directions, respectively. $P(z,k_x,k_y)=\mathrm{i}k\exp((-0.5/(kL))\times\mathrm{i}z(L-z)(k_x^2+k_y^2))$, $\Phi_\mathrm{n}(k)$ represents the refractive index spatial power spectrum of ocean turbulence[17], which is expressed as

$$\Phi_\mathrm{n}(k)=0.388\times10^{-8}u_xu_y\omega^{-2}\varepsilon^{-\frac{1}{3}}\chi_\mathrm{T}u^{-\frac{11}{6}}\cdot(1+2.35\nu^{\frac{1}{2}}\varepsilon^{-\frac{1}{6}}u^{\frac{1}{3}})[\omega^2\mathrm{e}^{-A_\mathrm{T}\delta}+\mathrm{e}^{-A_\mathrm{S}\delta}-2\omega\mathrm{e}^{-A_\mathrm{TS}\delta}] \quad (10)$$

where $u=(u_xk_x)^2+(u_yk_y)^2$, $A_\mathrm{T}=1.863\times10^{-2}$, $A_\mathrm{S}=1.9\times10^{-4}$, $A_\mathrm{TS}=9.41\times10^{-3}$, $\delta=8.284\nu\varepsilon^{-1/3}u^{2/3}+12.978\nu^{3/2}\varepsilon^{-1/2}u$. u_x and u_y denote the anisotropy factors in the x and y directions in ocean turbulence, respectively. The kinetic viscosity coefficient ν ranges from 10^{-5} $\mathrm{m^2/s}$ to 0 $\mathrm{m^2/s}$. The ratio of temperature to salinity contribution to ocean turbulence ω ranges from -5 to 0. The turbulence kinetic energy dissipation rate ε ranges from 10^{-10} $\mathrm{m^2/s^3}$ to 10^{-1} $\mathrm{m^2/s^3}$. The mean square temperature dissipation rate χ_T ranges from 10^{-10} $\mathrm{m^2/s^3}$ to 10^{-2} $\mathrm{m^2/s^3}$.

3.3 Pointing error

As shown in Fig. 3, when the beam arrives at the receiver at a distance L from the transmitting end, its beam width is w_z, and the receiving aperture radius is $R=D/2$. The attenuation coefficient caused by the pointing error is[18]

$$h_\mathrm{p}(r,L)=A_0\mathrm{e}^{-\frac{2r^2}{w_{z_\mathrm{eq}}}} \quad (11)$$

where r is the radial deviation, $A_0=[\varepsilon(\nu)]^2$ is the received optical power at the radial distance of zero, where $\varepsilon(\cdot)$ is error function, $\nu=\sqrt{\pi}R/(\sqrt{2}w_z)$, $w_{z_\mathrm{eq}}^2=w_z^2\sqrt{\pi}\varepsilon(\nu)/(2\nu\exp(-\nu^2))$ denotes the equivalent beamwidth, and w_z/R denotes the normalized beamwidth. The radial deviation r follows the Rayleigh distribution, and the probability density function of the pointing error is

$$f_{h_\mathrm{p}}(h_\mathrm{p})=\frac{\gamma^2}{A_0^{\gamma^2}}h_\mathrm{p}^{\gamma^2-1};\quad 0\leqslant h_\mathrm{p}\leqslant A_0 \quad (12)$$

where $\gamma=w_{z_\mathrm{eq}}/(2\sigma_\mathrm{s})$ represents the ratio of the equivalent beam radius at the receiving end to the standard deviation of the pointing error displacement, and σ_s is the random jitter error.

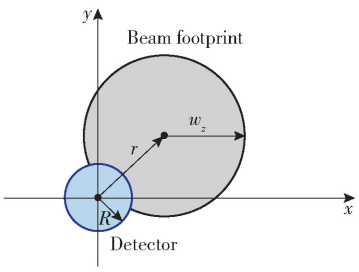

Fig. 3 Deflection of the beam in the receiving plane

3.4 Composite channel model

Optical signals transmitted in seawater are influenced by seawater attenuation, ocean turbulence, and pointing error, resulting in serious energy attenuation. In this paper, the effects of attenuation, turbulence, and pointing error introduced in the previous subsection are considered comprehensively. At this point, the composite channel attenuation factor can be expressed as

$$h_m=h_\mathrm{l}h_\mathrm{o}h_\mathrm{p} \quad (13)$$

where h_l represents the transmission path loss factor. h_o denotes the turbulence effect attenuation factor, and h_p

is the attenuation due to pointing error. These influencing factors are assumed to be statistically independent. Accordingly, the probability density function of the fading state of the UWOC composite channel is

$$f_{h_m}(h_m)=\frac{2\gamma^2(\alpha\beta)^{2(\alpha+\beta)}h^{\gamma^2-1}}{(A_0h_1)^{\gamma^2}\Gamma(\alpha)\Gamma(\beta)}\cdot\int_{\frac{h}{A_0h_1}}^{\infty}h_o^{\frac{\alpha+\beta}{2}-1-\gamma^2}\mathrm{K}_{\alpha-\beta}(2\sqrt{\alpha\beta h_o})\,\mathrm{d}h_o \tag{14}$$

$\mathrm{K}_{\alpha-\beta}(\cdot)$ can be expressed in terms of the Meijer G-function as

$$K_{\alpha-\beta}(x)=\frac{1}{2}G_{0,2}^{2,0}\left[\frac{x^2}{4}\,\middle|\,\frac{\alpha-\beta}{2},-\frac{\alpha-\beta}{2}\right] \tag{15}$$

Using Eq. (15), according to Ref. [19], Eq. (14) can be simplified as

$$f_{h_m}(h_m)=\frac{\alpha_m\beta_m\gamma^2}{A_0h_{l,m}\Gamma(\alpha_m)\Gamma(\beta_m)}\cdot G_{1,3}^{3,0}\left[\frac{\alpha_m\beta_m}{A_0h_1}h_m\,\middle|\,\begin{matrix}\gamma^2\\ \gamma^2-1,\alpha_m-1,\beta_m-1\end{matrix}\right] \tag{16}$$

From the simplified expression, the cumulative density function (CDF) can be obtained from $F_h(h)\triangleq\int_0^h f_h(h)\,\mathrm{d}h$ as

$$F_{h_m}(h_m)=\frac{\gamma^2}{\Gamma(\alpha_m)\Gamma(\beta_m)}G_{2,4}^{3,1}\left[\frac{\alpha_m\beta_m}{A_0h_{1,m}}h_m\,\middle|\,\begin{matrix}1,\gamma^2+1\\ \gamma^2,\alpha_m,\beta_m,0\end{matrix}\right] \tag{17}$$

where h denotes the attenuation coefficient.

4 Outage probability and average SER

4.1 Outage probability

If phase noise is not considered, the instantaneous signal-to-noise ratio (SNR) of the OFDM system can be expressed as $R_{\mathrm{SN}}(h)=2P_0h^2/(q\eta)=\bar{R}_{\mathrm{SN}}h^2$, where P_0 is the power of the signal light. Here, q denotes the electronic charge, η denotes the detector efficiency, $\bar{R}_{\mathrm{SN}}$ denotes the average SNR, $\bar{R}_{\mathrm{SN}}=2P_0/(q\eta)$. The outage probability refers to the probability that the instantaneous SNR at the receiver falls below a predetermined threshold value, denoted as $R_{\mathrm{SN,th}}$. This is expressed as

$$P_{\mathrm{out}}=\Pr(R_{\mathrm{SN}}(h)\leqslant R_{\mathrm{SN,th}})=\int_h f_h(h)\,\mathrm{d}h \tag{18}$$

Assuming the m channels are statistically independent, the total outage probability corresponding to the m channels can be derived and is given by

$$P_{\mathrm{out},M}=\prod_{m=1}^{M}\Pr(R_{\mathrm{SN}}(h_m)\leqslant R_{\mathrm{SN,th}})=\Pr(\bar{R}_{\mathrm{SN}}h^2\leqslant R_{\mathrm{SN,th}})=\prod_{m=1}^{M}F_m\left(\sqrt{\frac{R_{\mathrm{SN,th}}}{\bar{R}_{\mathrm{SN}}}}\right) \tag{19}$$

By substituting Eq. (17) into Eq. (19), the total outage probability of UWOC system based on OFDM-QPSK modulation with wavelength diversity can be expressed as

$$P_{\mathrm{out},M}=\prod_{m=1}^{M}\frac{\gamma^2}{\Gamma(\alpha_m)\Gamma(\beta_m)}\cdot G_{2,4}^{3,1}\left[\frac{\alpha_m\beta_m}{A_0h_{1,m}}\sqrt{\frac{R_{\mathrm{SN,th}}}{\bar{R}_{\mathrm{SN}}}}\,\middle|\,\begin{matrix}1,\gamma^2+1\\ \gamma^2,\alpha_m,\beta_m,0\end{matrix}\right] \tag{20}$$

4.2 Average SER

In UWOC system, when OFDM modulation is used at the transmitter side with QPSK mapping, the SER of the system can be expressed as[20]

$$P_{\mathrm{s}}=Q\left(\sqrt{\bar{R}_{\mathrm{SN}}h^2\frac{2TB}{S}}\right) \tag{21}$$

where $Q(\cdot)$ is the Gaussian Q-function, $\bar{R}_{\mathrm{SN}}$ represents the average SNR, T is the symbol period, S is the number of subcarriers of the OFDM signal, B denotes the signal bandwidth.

4.2.1 MRC

In wavelength diversity OFDM underwater wireless communication system using the MRC technique, the signals on each receiving path are combined with in-phase weighting. The path with the strongest signal is assigned the highest weight. The average SER of the system can be expressed as

$$P_{\mathrm{avs,MRC}}=\int_0^{\infty}Q\left(\sqrt{\frac{2TB\bar{R}_{\mathrm{SN}}}{MS}\sum_{m=1}^{M}h_m^2}\right)f_{h_m}(h_m)\,\mathrm{d}h_m \tag{22}$$

where h_m denotes different channel fading states. Using $Q(x)\approx(1/12)\exp(-x^2/2)+(1/4)\exp(-2x^2/3)$, $\exp(-x)=G_{0,1}^{1,0}(x\,|\,{}_0^-)$ and Eq. (21) in Ref. [21], Eq. (22) can be simplified to derive the final MRC average mis-sign expression, shown as

$$P_{\text{avs,MRC}}=\frac{1}{12}\prod_{m=1}^{M}\frac{2^{\alpha_m+\beta_m-3}\gamma^2}{\Gamma(\alpha_m)\Gamma(\beta_m)\pi}G_{6,3}^{1,6}\left[\frac{16TB\bar{R}_{\text{SN}}A_0^2h_{1,m}^2}{\alpha_m^2\beta_m^2MS}\middle|\begin{matrix}\frac{1-\gamma^2}{2},\frac{2-\gamma^2}{2},\frac{1-\alpha_m}{2},\frac{2-\alpha_m}{2},\frac{1-\beta_m}{2},\frac{2-\beta_m}{2}\\0,\frac{\gamma^2}{2},\frac{\gamma^2+1}{2}\end{matrix}\right]+$$
$$\frac{1}{4}\prod_{m=1}^{M}\frac{2^{\alpha_m+\beta_m-3}\gamma^2}{\Gamma(\alpha_m)\Gamma(\beta_m)\pi}G_{6,3}^{1,6}\left[\frac{64TB\bar{R}_{\text{SN}}A_0^2h_{1,m}^2}{3\alpha_m^2\beta_m^2MS}\middle|\begin{matrix}\frac{1-\gamma^2}{2},\frac{2-\gamma^2}{2},\frac{1-\alpha_m}{2},\frac{2-\alpha_m}{2},\frac{1-\beta_m}{2},\frac{2-\beta_m}{2}\\0,\frac{\gamma^2}{2},\frac{\gamma^2+1}{2}\end{matrix}\right] \tag{23}$$

4.2.2 EGC

EGC sets all the variable weights in the MRC technique to the same value and then performs the same operation as in the MRC scheme to sum the signals in-phase. Since EGC does not require different weights for each channel, it reduces system complexity compared to the MRC technique and simplifies the experimental equipment. The expression for the average SER when using the EGC technique can be derived similarly to that for the MRC technique, shown as

$$P_{\text{avs,EGC}}=\int_0^{\infty}Q\left[\sqrt{\frac{2\bar{R}_{\text{SN}}TB}{M^2S}\left(\sum_{m=1}^{M}h_m\right)^2}\right]f_{h_m}(h_m)\,\mathrm{d}h_m \tag{24}$$

Simplifying Eq. (24) leads to the final expression for the EGC average SER shown as

$$P_{\text{avs,EGC}}=\frac{1}{12}\prod_{m=1}^{M}\frac{2^{\alpha_m+\beta_m-3}\gamma^2}{\Gamma(\alpha_m)\Gamma(\beta_m)\pi}G_{6,3}^{1,6}\left[\frac{16TB\bar{R}_{\text{SN}}A_0^2h_{1,m}^2}{\alpha_m^2\beta_m^2M^2S}\middle|\begin{matrix}\frac{1-\gamma^2}{2},\frac{2-\gamma^2}{2},\frac{1-\alpha_m}{2},\frac{2-\alpha_m}{2},\frac{1-\beta_m}{2},\frac{2-\beta_m}{2}\\0,\frac{\gamma^2}{2},\frac{\gamma^2+1}{2}\end{matrix}\right]+$$
$$\frac{1}{4}\prod_{m=1}^{M}\frac{2^{\alpha_m+\beta_m-3}\gamma^2}{\Gamma(\alpha_m)\Gamma(\beta_m)\pi}G_{6,3}^{1,6}\left[\frac{64TB\bar{R}_{\text{SN}}A_0^2h_{1,m}^2}{3\alpha_m^2\beta_m^2M^2S}\middle|\begin{matrix}\frac{1-\gamma^2}{2},\frac{2-\gamma^2}{2},\frac{1-\alpha_m}{2},\frac{2-\alpha_m}{2},\frac{1-\beta_m}{2},\frac{2-\beta_m}{2}\\0,\frac{\gamma^2}{2},\frac{\gamma^2+1}{2}\end{matrix}\right] \tag{25}$$

5 Experimental results and analysis

This section analyzes the performance of the system using wavelength diversity UWOC under pointing error and ocean turbulence, based on the analytical expressions for the outage probability and the average SER derived from the previous theoretical derivations. The system simulation is conducted using Matlab. The simulation parameters are provided in Table 2.

Table 2 Simulation parameter

Parameter	Value
Ratio of temperature and salinity contribution to ocean turbulence ω	−1
Kinetic energy dissipation rate $\varepsilon/(\mathrm{m}^2\cdot\mathrm{s}^{-3})$	10^{-4}
Mean square temperature dissipation rate $\chi_{\text{T}}/(\mathrm{K}^2\cdot\mathrm{s}^{-1})$	10^{-4}
Dynamic viscosity coefficient $\nu/(\mathrm{m}^2\cdot\mathrm{s}^{-1})$	10^{-5}
Receiver diameter D/mm	1
Transmission distance L/m	10
Ratio of beam width to aperture radius w_z/R	4
Ratio of jitter standard deviation variance to aperture radius σ_s/R	3
Wavelength/nm	560,570,580
Photon detection efficiency η/%	32,30,29
Modulation order	4
Signal bandwidth/MHz	6.4
Subcarrier spacing/kHz	25
Number of subcarrier	256

The receiver responsivity is calculated as $\rho = G\eta e/(h\nu)$, where e denotes the electron charge, h denotes Planck's constant, ν denotes the frequency, G denotes the multiplication factor of avalanche photodiode, and η denotes the photon detection efficiency. The photon detection efficiencies at the wavelengths 560 nm, 570 nm, and 580 nm are 32%, 30%, and 29%, respectively. The average SNR of optical signals at wavelengths of 560 nm, 570 nm and 580 nm transmitted in seawater are $\overline{R}_{SN1}$, $\overline{R}_{SN2}$ and $\overline{R}_{SN3}$, respectively. When L = 10 m, the average SNR of optical signals at wavelength 560 nm is $\overline{R}_{SN2} = 0.946\overline{R}_{SN1}$, and at 580 nm is $\overline{R}_{SN3} = 0.778\overline{R}_{SN1}$. When L = 15 m, the average SNR of 560 nm is $\overline{P}_{SN2} = 0.895\overline{R}_{SN1}$, and at 580 nm is $\overline{R}_{SN3} = 0.704\overline{R}_{SN1}$.

Fig. 4 shows the variation in the outage probability with normalized SNR for the UWOC system transmitting under strong turbulence with pointing errors of 2, 3, and 4, respectively. When $u_x = 2, u_y = 2$, the Rytov variance exceeds 1, indicating that the system operates in a strongly turbulent environment.

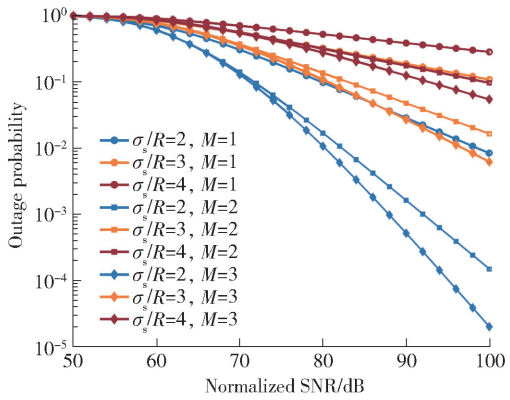

Fig. 4 Variation of the outage probability of the wavelength diversity UWOC system with normalized SNR under different pointing errors

In Fig. 4, the system with wavelength diversity demonstrates a lower outage probability than the system without wavelength diversity when the pointing error is constant. Furthermore, the performance of the 3rd-order wavelength diversity system is better than that of the 2nd-order wavelength diversity system. For instance, at SNR of 100 dB and $\sigma_s/R = 2$, the outage probabilities are 8.328×10^{-3}, 1.475×10^{-4}, and 1.969×10^{-5} for M = 1, 2, and 3, respectively. Additionally, for the same diversity order, the average SER decreases gradually with decreasing pointing error. The outage probability of the system decreases from 0.095 to 1.475×10^{-4} when the SNR of 100 dB.

Fig. 5 investigates the variation in outage probability with normalized SNR when the ratio of beam width to aperture radius is 4, 6, and 8, respectively. In Fig. 5, the larger the ratio of beam width to aperture radius, the smaller the beam drift, resulting in a more stable signal received at the receiver and thus reducing the system outage probability. For example, at SNR of 100 dB and w_z/R increases from 4 to 8, the outage probability decreases from 0.108 to 5.289×10^{-4} in the no-wavelength diversity system. In contrast, in the 3rd-order wavelength diversity system, the outage probability decreases from 6.086×10^{-3} to 5.138×10^{-8}.

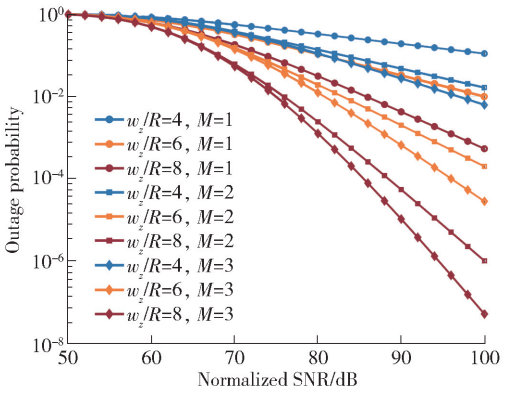

Fig. 5 Variation of the outage probability of the wavelength diversity UWOC system with normalized SNR under different beam width to aperture radius ratios

Fig. 6 plots the variation in the average SER of the wavelength diversity UWOC system using MRC and EGC techniques at the receiver side when transmitting over 10 m in isotropic and anisotropic strong ocean turbulence conditions. In Fig. 6 (b), when SNR is 30 dB, the average SER of the 2nd-order and 3rd-order wavelength diversity UWOC systems using MRC technology in anisotropic turbulent conditions are 5.528×10^{-5} and 2.23×10^{-6}, respectively. For the 2nd-order and 3rd-order wavelength diversity UWOC system using EGC technology, the average SER are 8.018×10^{-5} and 6.116×10^{-6}, respectively. The results show that the average SER of the UWOC system

using 2nd-order and 3rd-order wavelength diversity decreases in turbulent conditions compared to a system without wavelength diversity. As the number of operating wavelengths increases, the average SER of the system decreases more significantly. Additionally, the MRC technique at the receiver side in the UWOC system with the same number of diversity orders results in a lower average SER than the EGC technique.

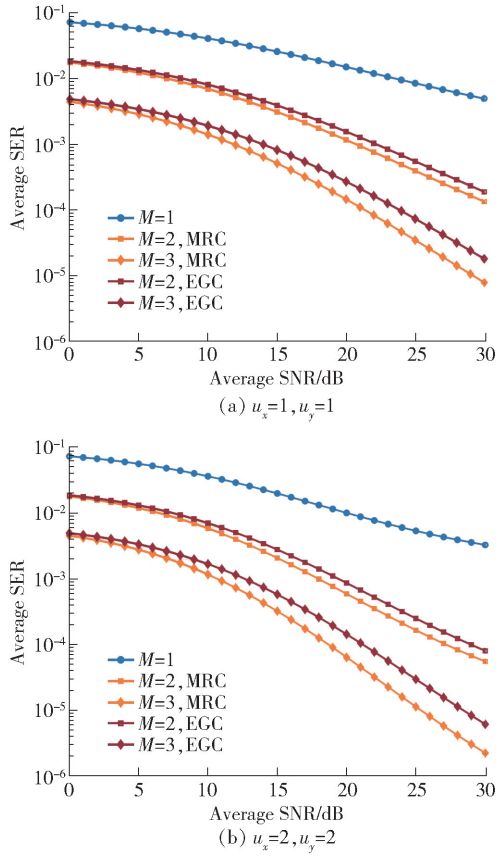

Fig. 6 Comparison of average SER of the wavelength diversity UWOC systems using MRC and EGC techniques with different anisotropy factors

Fig. 7 investigates the impact of the number of subcarriers on the average SER of the wavelength diversity UWOC system at transmission distances of 10 m and 15 m. Analysis of Fig. 7 reveals that, under the same diversity order and SNR conditions, the system achieves a lower SER when the number of subcarriers is 128. In Fig. 7(a), with $M=3$ and SNR of 70 dB, the average SER is 4.492×10^{-5} for 128 subcarriers and 6.625×10^{-5} for 256 subcarriers. This indicates that increasing the number of subcarriers results in a higher average SER, with a more noticeable impact on systems utilizing diversity. The number of subcarriers is not always better when increased, as modulating multiple subcarriers with the same phase signal may lead to significant peak power after aggregation. The more subcarriers there are, the higher the aggregated signal peak, potentially causing inter-carrier interference and degrading system performance. When the transmission distance increases to 15 m, the average SER of a non-diversity system with 128 subcarriers increases from 5.516×10^{-3} to 8.757×10^{-3}; in a 2nd-order diversity system, it increases from 2.447×10^{-4} to 9.527×10^{-4}; and in a 3rd-order diversity system, it increases from 4.492×10^{-5} to 2.402×10^{-4}. Therefore, while the system's communication coverage expands with increased transmission distance, the average SER also increases. Thus, using wavelength diversity technology and selecting an appropriate number of subcarriers can improve system performance.

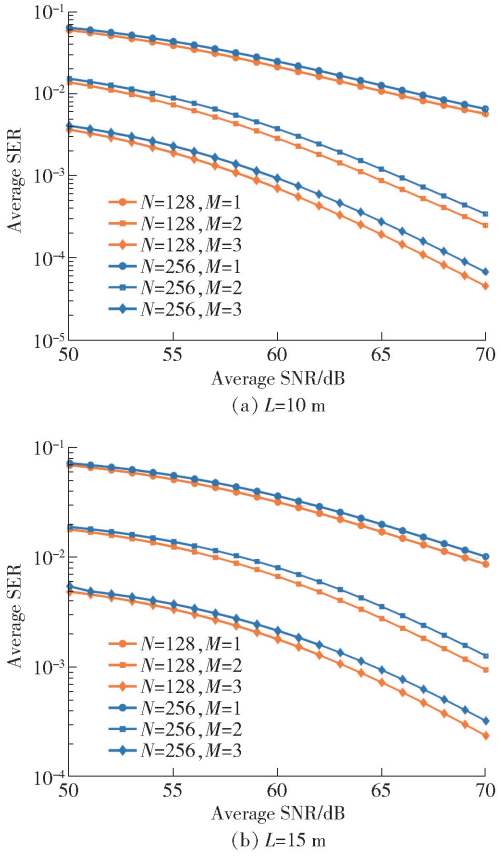

Fig. 7 Variation of the average SER with the average SNR under different transmission distances and subcarrier numbers

Fig. 8 shows the performance variation in the average SER of the wavelength diversity UWOC system under different anisotropy factors.

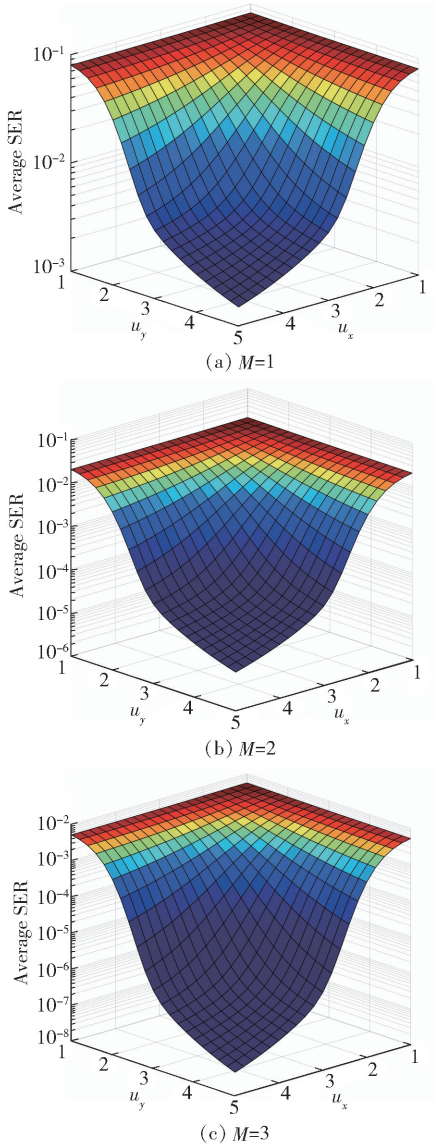

Fig. 8 Comparison of average SER performance of wavelength diversity systems with different anisotropy factors

As the anisotropy factors u_x and u_y increase simultaneously in the x and y directions, respectively, the average SER of the UWOC systems without wavelength diversity and with 2nd-order and 3rd-order wavelength diversity decrease significantly, and are symmetrically distributed. For example, in the 3rd-order wavelength diversity UWOC system, increasing the anisotropy factors u_x and u_y causes the average SER to decrease from 5.597×10^{-3} to 4.487×10^{-8}. When the anisotropy factors are equal, the average SER of the system using wavelength diversity is lower compared to the system without wavelength diversity. Additionally, the 3rd-order wavelength diversity UWOC system performs better than the 2nd-order UWOC system. At the anisotropy factor $u_x = 3, u_y = 4$, the average SER of the no-wavelength diversity UWOC system is 5.993×10^{-3}, while the average SER of the 2nd-order and 3rd-order wavelength diversity UWOC systems are 1.508×10^{-4} and 5.985×10^{-6}, respectively.

6 Conclusions

In this paper, a wavelength diversity-based OFDM-QPSK UWOC system was proposed, which comprehensively considers the effects of attenuation, turbulence, and pointing error during optical signal transmission. An underwater composite channel model is established, and analytical expressions for the outage probability and average SER are derived based on equivalent structural parameters expressed by ocean refractive index fluctuations and the anisotropy factor. These expressions are used to analyze the performance variations of wavelength diversity UWOC under different conditions. The results show that, compared with the UWOC system without wavelength diversity, the system using wavelength diversity technique has improved outage probability and average SER. As the anisotropy factor increases, the impact of ocean turbulence on the system gradually diminishes. The higher the diversity order, the average SER gradually decreases, with values as low as 4.487×10^{-8}. For the same order of wavelength diversity, the average SER of the system using MRC at the receiver side is lower than that using EGC, while the system is more complicated than the experimental system. Furthermore, reducing the pointing error decreases the system's outage probability. When the diversity order is 3, reducing the pointing error from 4 to 2 decreases the outage probability from 5.384×10^{-2} to 1.969×10^{-5}. In OFDM systems, increasing the number of subcarriers does not always enhance performance, it

depends on the specific channel environment and system parameter settings. This paper provides a theoretical foundation for the subsequent design and optimization of OFDM systems.

Acknowledgements

This work was supported by the Equipment Pre Research Joint Fund Funded Project by the Ministry of Education of China (8091B032130).

References

[1] KAUSHAL H, KADDOUM G. Underwater optical wireless communication. IEEE Access, 2016, 4: 1518 – 1547.

[2] STASSINAKIS A N, NISTAZAKIS H E, VAROTSOS G K, et al. Performance of underwater wireless optical link under weak turbulence and pointing errors using heterodyne QAM technique. Proceedings of the 23th International IFIP Conference on Optical Network Design and Modeling (ONDM'19), 2019, May 13 – 16, Athens, Greece. LNCS 11616. Cham, Switzerland: Springer Nature Switzerland AG, 2019: 552 – 559.

[3] YI X, LI Z, LIU Z J. Underwater optical communication performance for laser beam propagation through weak oceanic turbulence. Applied Optics, 2015, 54 (6): 1273 – 1278.

[4] HE F T, DU Y, ZHANG J L, et al. Bit error rate of pulse position modulation wireless optical communication in gamma-gamma oceanic anisotropic turbulence. Acta Physica Sinica, 2019, 68(16): 236 – 244 (in Chinese).

[5] SRIVASTAVA V, MANDLOI A, SONI G G. Outage probability and average BER estimation of FSO system employing wavelength diversity. Optical and Quantum Electronics, 2019, 51 (7): Article 229.

[6] WANG Y, ZHU L, FENG W K. Performance study of wavelength diversity serial relay OFDM FSO system over exponentiated Weibull channels. Optics Communications, 2021, 478: Article 126470.

[7] HE F T, LI J Q, ZHANG J L, et al. Performance analysis of wavelength diversity wireless optical communication system in ocean turbulence. Infrared and Laser Engineering, 2021, 50(12): 1 – 10 (in Chinese).

[8] NAYAK N, KESWANI B, NAYAK D R, et al. Performance evaluation of DP-QPSK modulation for underwater optical wireless communication using a green light propagation. Proceedings of the 2022 OITS International Conference on Information Technology (OCIT'22), 2022, Dec 14 – 16, Bhubaneswar, India. Piscataway, NJ, USA: IEEE, 2022: 428 – 432.

[9] MOHAMMED A, ABD H J. Performance assessment of underwater optical wireless based on QPSK-OFDM. Proceedings of the 2nd International Conference on Advances in Engineering Science and Technology (AEST'22), 2022, Oct 24 – 25, Babil, Iraq. Piscataway, NJ, USA: IEEE, 2022: 389 – 393.

[10] SRIVASTAVA V, MANDLOI A, PATEL D. Analysis of outage probability in wavelength diversity based FSO link under gamma-gamma fading with varying atmospheric attenuation. Wireless Personal Communications, 2021, 116(3): 1933 – 1947.

[11] YAO Y X. Research on QAM-OFDM underwater wireless optical communication system based on LED array light source. Master Thesis. Dalian, China: Dalian University of Technology, 2022 (in Chinese).

[12] HEMA R, SUDHA S, AARTHI K. Performance studies of MIMO based DCO-OFDM in underwater wireless optical communication systems. Journal of Marine Science and Technology, 2021, 26(1): 97 – 107.

[13] WANG F, YANG Y, DUAN Z L, et al. Characteristic analysis of underwater laser transmission channel based on visible light. Optical Communication Technology, 2016, 40(3): 26 – 28 (in Chinese).

[14] FU Y Q, DU Y Z. Performance of heterodyne differential phase shift-keying underwater wireless optical communication systems in gamma-gamma-distributed turbulence. Applied Optics, 2018, 57(9): 2057 – 2063.

[15] FU Y Q, HUANG C T, DU Y Z. Effect of aperture averaging on mean bit error rate for UWOC system over moderate to strong oceanic turbulence. Optics Communications, 2019, 451: 6 – 12.

[16] BAYKAL Y. Scintillation index in strong oceanic turbulence. Optics Communications, 2016, 375: 15 – 18.

[17] ZOU Z X, WANG P, CHEN W W, et al. Average capacity of a UWOC system with partially coherent Gaussian beams propagating in weak oceanic turbulence. Journal of the Optical Society of America A, 2019, 36(9): 1463 – 1474.

[18] FU Y Q, DUAN Q, ZHOU L. Performance of underwater wireless optical communication system in gamma gamma strong oceanic turbulence with pointing error. Infrared and Laser Engineering, 2020, 49(2): 98 – 105 (in Chinese).

[19] GRADSHTEYN I S, RYZHIK I M. Table of integrals, series, and products. 7th ed. New York, NY, USA: Academic, 2008.

[20] ZHU Z Y, WU H, WANG Y. Performance study of serial relay OFDM FSO system under QPSK modulation. Proceedings of SPIE 11341, the 8th Applied Optics and Photonics China: Space Optics, Telescopes, and Instrumentation (AOPC'2019), 2019, Jul 7 – 9, Beijing, China. Bellingham, WA, USA: SPIE, 2019: 113410Y.

[21] ADAMCHIK V S, MARICHEV O I. The algorithm for calculating integrals of hypergeometric type functions and its realization in REDUCE system. Proceedings of the 1990 International Symposium on Symbolic and Algebraic Computation (ISSAC'90), 1990, Aug 20 – 24, Tokyo, Japan. New York, NY, USA: ACM, 1990: 212 – 224.

(Editor: Wang Xuying)